Electronic Supplementary Material (ESI) for Journal of Materials Chemistry C.

SUPPORTING INFORMATION

Dielectric behaviour of nitrogen doped perovskite $SrTiO_{3-\delta}N_{\delta}$ films

M. Tyunina,*[ab] L. L. Rusevich,[c]* M. Savinov,[b] E. A. Kotomin,[cd] A. Dejneka [b]

[a] *Microelectronics Research Unit, Faculty of Information Technology and Electrical Engineering, University of Oulu, P. O. Box 4500, FI-90014 Oulu, Finland*

[b] *Institute of Physics of the Czech Academy of Sciences, Na Slovance 2, 18221 Prague, Czech Republic*

[c] *Institute of Solid State Physics, University of Latvia, Kengaraga Str. 8, LV-1063 Riga, Latvia*

[d] *Max Planck Institute for Solid State Research, Heisenberg Str. 1, Stuttgart D-70569, Germany*

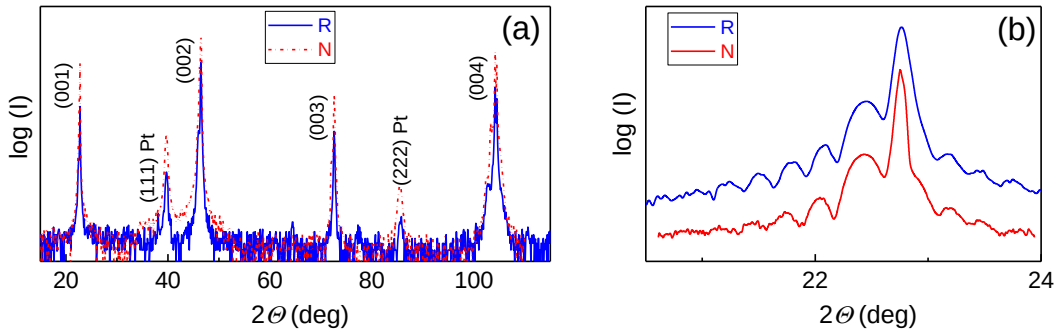

Fig. S1. X-ray (Cu Kα) diffraction Θ-2Θ scans in the regular (R) and nitrogen-doped (N) STO films grown on $SrRuO_3$-coated (001) STO substrates and with the Pt top electrodes. In (a), perovskite (00l) diffractions and diffractions from Pt are marked. In (b), details of the scans around (001) diffractions are shown. The Laue satellites are from the 40-nm-thick epitaxial bottom electrode layer of $SrRuO_3$.

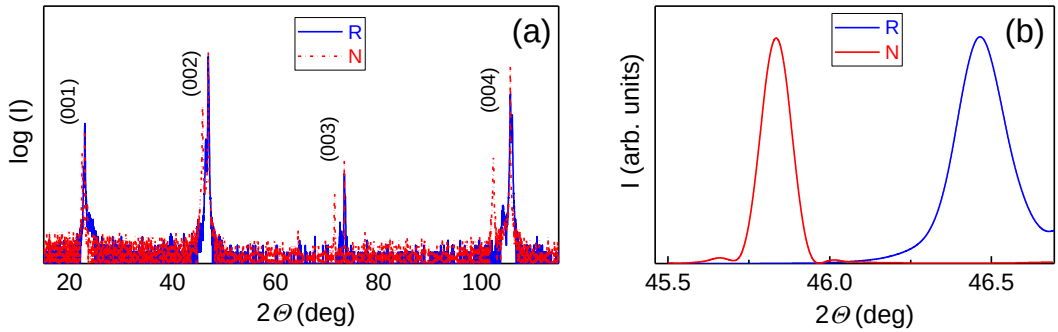

Fig. S2. X-ray (Cu Kα) diffraction Θ-2Θ scans in the regular (R) and nitrogen-doped (N) STO films grown on $LaNiO_3$-coated (001) LSAT substrates. In (a), perovskite (00l) diffractions are marked. In (b), details of the scans around (002) diffractions are shown.

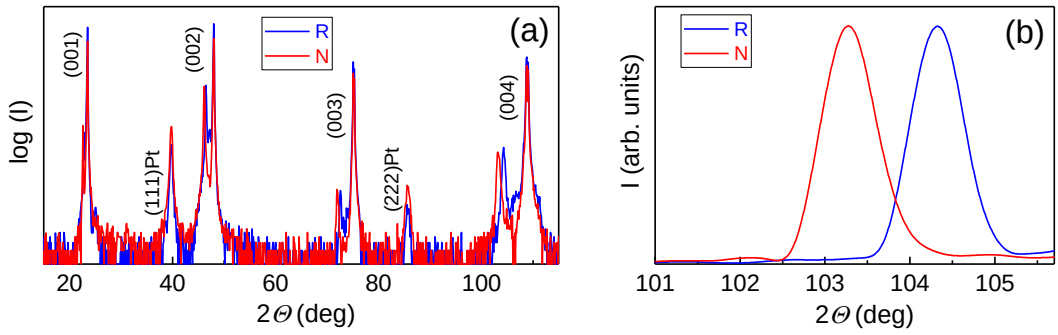

Fig. S3. X-ray (Cu Kα) diffraction Θ-2Θ scans in the regular (R) and nitrogen-doped (N) STO films grown on $LaNiO_3$-coated (001) LAO substrates and with the Pt top electrodes. In (a), perovskite (00l) diffractions and diffractions from Pt are marked. In (b), details of the scans around (002) diffractions are shown.

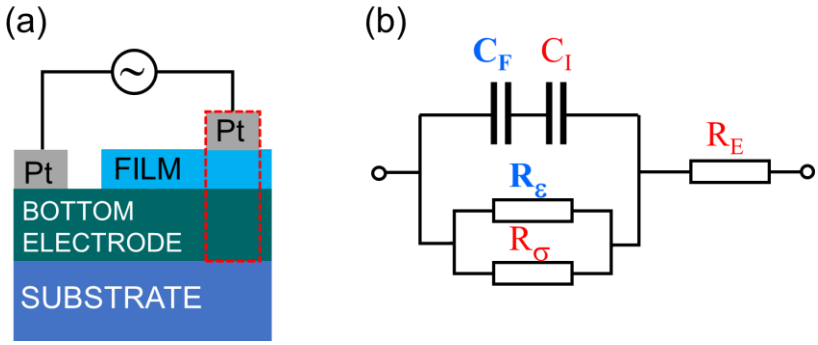

Fig. S4. (a) Schematics of cross-section and (b) equivalent circuit of the vertical thin-film capacitor.

Equivalent-circuit model:
Z^* - complex impedance of the capacitor
C_F – capacitance of the film
C_I – capacitance of a thin low-permittivity layer at the film-electrode interfaces, or interfacial capacitance
R_ε – resistance, which is determined by the dielectric losses of the film
R_σ – resistance, which is determined by the charge transport in the film
R_E – resistance of the thin electrode layers
$\omega = 2\pi f$, where f is the frequency

$$Z^* = R - iX = \left[R_E + \frac{R_F}{1+(\omega C R_F)^2}\right] - i\left[\frac{\omega C R_F^2}{1+(\omega C R_F)^2}\right] \quad \text{(S1)}$$

$$\frac{1}{R_F} = \frac{1}{R_\varepsilon} + \frac{1}{R_\sigma} \quad \text{(S2)}$$

$$\frac{1}{C} = \frac{1}{C_F} + \frac{1}{C_I} \quad \text{(S3)}$$

The measured capacitance C_p is approximated by

$$C_p \approx \frac{X}{\omega(X^2+R^2)} \quad \text{(S4)}$$

The real part of the dielectric permittivity ε is calculated from the measured capacitance:

$$C_p = \frac{\varepsilon_0 \varepsilon S}{d} \quad \text{(S5)}$$

Here d is the thickness of the film and S is the area of the top electrode and, hence, of the capacitor.

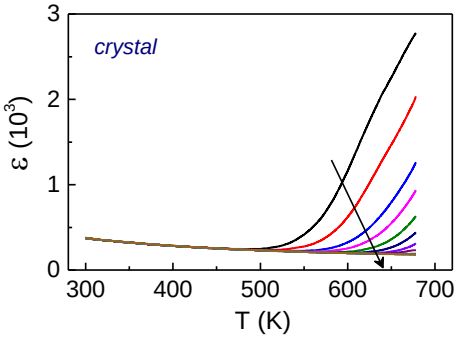

Fig. S5. The real part of the dielectric permittivity as a function of temperature at different frequencies f = 1-10^6 Hz in the reference STO crystal. Arrow shows direction of frequency increase.

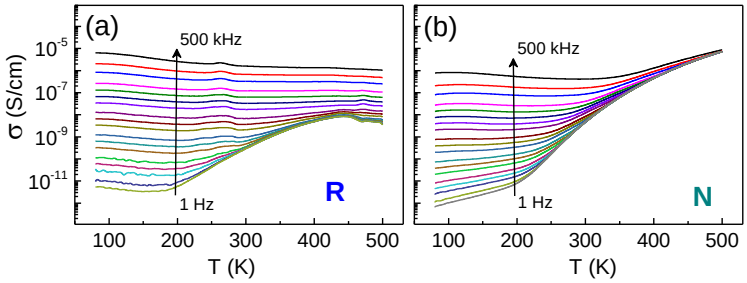

Fig. S6. The real part of conductivity as a function of temperature at different frequencies f = 1-10^6 Hz in the polycrystalline regular $SrTiO_3$ (R) and nitrogen doped $SrTiO_{2.7}N_{0.3}$ (N) films. Arrows show direction of frequency increase.

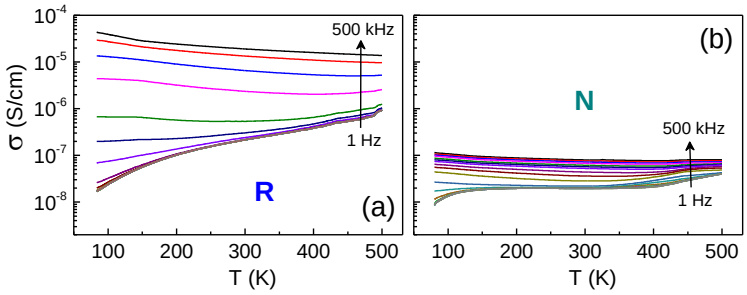

Fig. S7. The real part of conductivity as a function of temperature at different frequencies f = 1-10^6 Hz in the homoepitaxial regular $SrTiO_3$ (R) and nitrogen doped $SrTiO_{2.7}N_{0.3}$ (N) films. Arrows show direction of frequency increase.

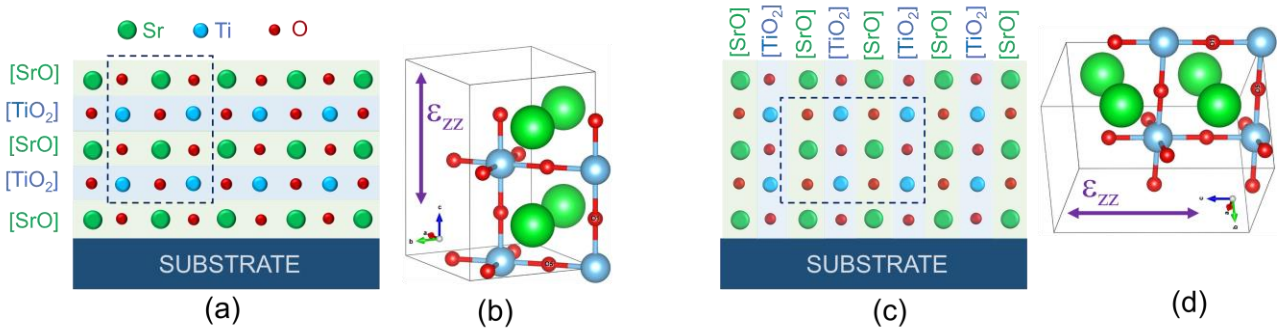

Fig. S8. (a, c) Schematics of atomic planes in epitaxial tetragonal (a) (001)-oriented and (c) (100)-oriented STO films. (b, d) Schematics of atomic positions in tetragonal (b) (001)-oriented and (d) (100) oriented STO cell. The atoms are shown by circles. The dielectric tensor component ε_{zz} is (b) out-of-plane or (d) in-plane.

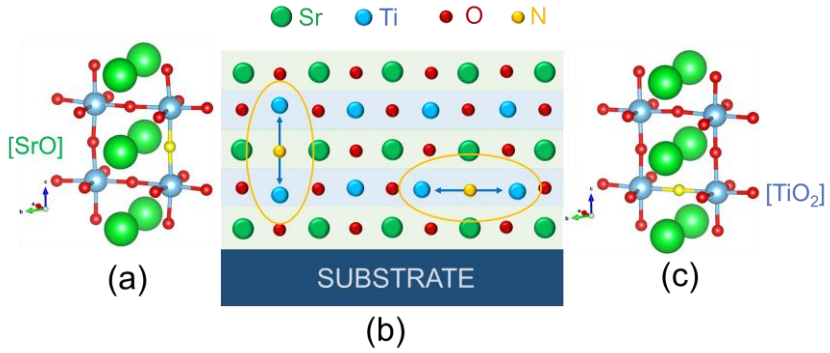

Fig. S9. Schematics of atomic planes and nitrogen-induced elastic dipoles in epitaxial (001) STO film. The dipoles are caused by elongation of the Ti-Ti distance and possess different crystallographic orientation for nitrogen in the (a) SrO- and (c) TiO_2- planes. The atoms are shown by circles, elongations are marked by arrows, and elastic dipoles are indicated by ellipses.

Table S1. Structural parameters of crystallographic unit cell in unstressed and in-plane compressed pure and nitrogen-doped STO. *a*, *b*, *c* — lattice constants; α, β, γ — angles between axes; *V* — unit cell volume.

	UNSTRESSED			IN-PLANE COMPRESSED		
	pure	N in SrO	N in TiO_2	pure	N in SrO	N in TiO_2
a, Å	5.489	5.502	5.516	5.433	5.433	5.433
b, Å	5.489	5.502	5.509	5.433	5.433	5.433
c, Å	7.775	7.828	7.790	7.841	7.904	7.941
α, deg	90.00	90.08	89.65	90	90	90
β, deg	90.01	89.92	90.27	90	90	90
γ, deg	90.00	89.24	89.50	90	90	90
V, $Å^3$	234.2	236.9	236.7	231.4	233.3	234.4

Table S2. Frequencies v and contributions $\Delta\varepsilon_{zz}$ to ε_{zz} component of the static dielectric tensor for the eight lowest-frequency TO modes in unstressed and in-plane compressed pure and nitrogen-doped STO.

UNSTRESSED						IN-PLANE COMPRESSED					
pure		N in SrO		N in TiO_2		pure		N in SrO		N in TiO_2	
ν, cm^{-1}	$\Delta\varepsilon_{zz}$	ν, cm^{-1}	$\Delta\varepsilon_{zz}$	ν, cm^{-1}	$\Delta\varepsilon_{zz}$	ν, cm^{-1}	$\Delta\varepsilon_{zz}$	ν, cm^{-1}	$\Delta\varepsilon_{zz}$	ν, cm^{-1}	$\Delta\varepsilon_{zz}$
16.78	0	49	17	23	13	75.871	0	84	0	71	7
16.80	0	51	0	*39*	*176*	75.872	0	*88*	*167*	86	0
52	4	*81.56*	*153*	75	0	*90*	*231*	92	0	94	0
53	9	82.45	12	86	1	99	0	111	0	99	2
57	*743*	86	22	88	40	120	33	114	0	113	2
68	1	116.9	0	104	53	121.86	0	119	0	120	0
89	0	117.3	0	108	24	121.88	0	120	0	122	0
114.89	0	118	0	114	47	123	0	122	0	123	0

Total ε_{zz} component is 760 (pure), 228 (N in SrO) and 368 (N in TiO_2) in unstressed STO and 266 (pure), 197 (N in SrO), and 56 (N in TiO_2) in compressed STO.

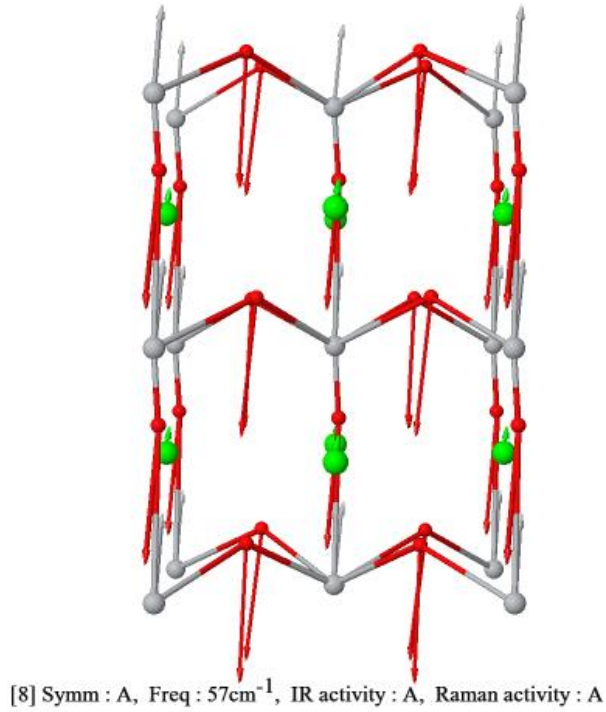

Fig. S10. Schematic presentation of atomic displacements in the mode with frequency 57 cm^{-1} for pure unstressed STO. View along *y*-axis. Sr — green balls, Ti — grey, oxygen — red.

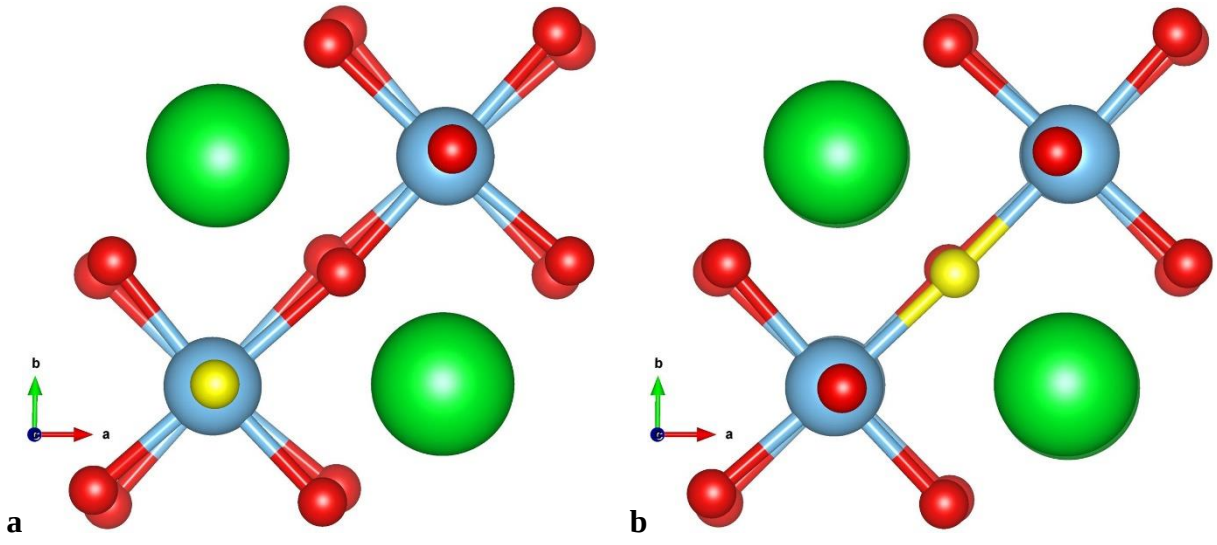

Fig. S11. Schematics of the structure of unstressed nitrogen doped STO. Sr atoms are shown by green balls, Ti atoms — blue balls, oxygen atoms — red balls, nitrogen atoms – yellow balls. The nitrogen substitution is (a) axial (in the SrO plane) and (b) equatorial (in the TiO_2 plane). View along z-axis (rotation of TiO_6 octahedra around *z*-axis).

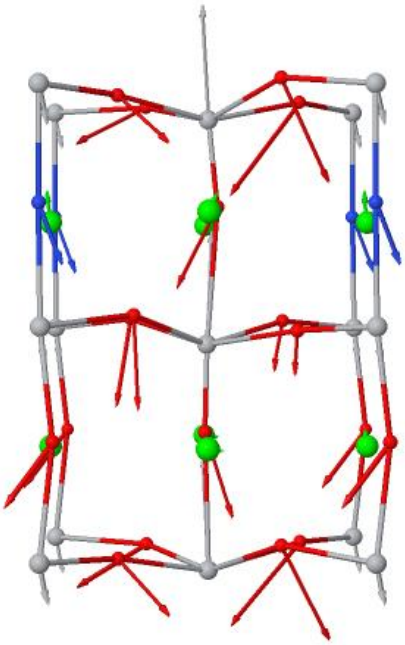

[6] Symm : A, Freq : 82cm^{-1}, IR activity : A, Raman activity : A

Fig. S12. Schematic presentation of atomic displacements in the mode with frequency 81.56 cm^{-1} for nitrogen substitution in the SrO plane in unstressed STO. View along the *y*-axis. Sr — green balls, Ti — grey, oxygen — red, nitrogen — blue.

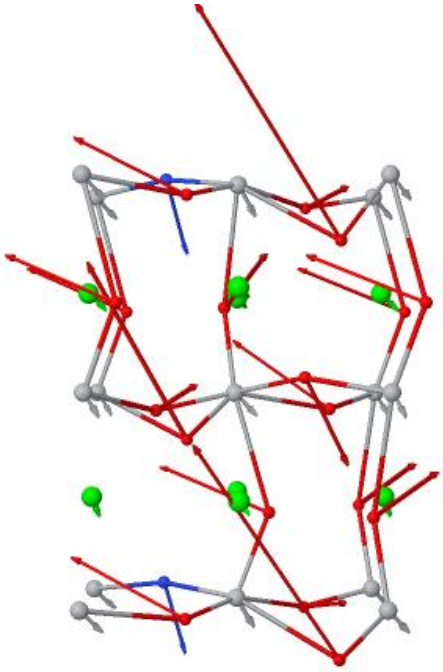

[5] Symm : A, Freq : 39cm^{-1}, IR activity : A, Raman activity : A

Fig. S13. Schematic presentation of atomic displacements in the mode with frequency 39 cm^{-1} for nitrogen substitution in the TiO_2 plane in unstressed STO. View along the *y*-axis. Sr — green balls, Ti — grey, oxygen — red, nitrogen — blue.

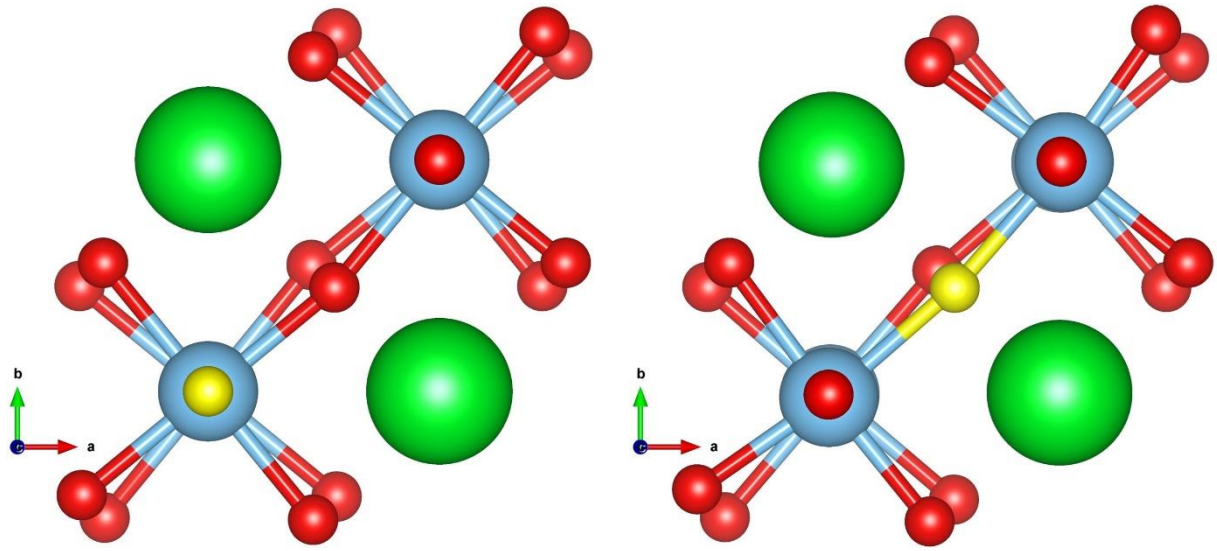

Fig. S14. Schematics of the structure of in-plane compressed nitrogen-doped STO. Sr atoms are shown by green balls, Ti atoms — blue balls, oxygen atoms — red balls, nitrogen atoms – yellow balls. The nitrogen substitution is (a) axial (in the SrO plane) and (b) equatorial (in the TiO_2 plane). View along z-axis (rotation of TiO_6 octahedra around *z*-axis).

Table S3. Lattice strain and dielectric constant in unstressed and in-plane compressed pure and nitrogen doped STO. s_a – in-plane strain, s_c – out-of-plane strain, ε_{zz} – out-of-plane component of the dielectric tensor.

	UNSTRESSED			IN-PLANE COMPRESSED		
	pure	N in SrO	N in TiO_2	pure	N in SrO	N in TiO_2
s_a, %	0	+0.2	+0.5	-1.0	-1.0	-1.0
s_c, %	0	+0.7	+0.2	+0.85	+1.7	+2.1
ε_{zz}	760	228	368	266	197	56